

A weak upper limit for axion-related continuum polarization signal at 630 nm

C. Beck¹

National Solar Observatory, Boulder/CO

Received xxx; accepted xxx

ABSTRACT

Context. Axions could be a component of the dark matter and are of great interest for particle physics. If present, their interaction with magnetic fields in the solar photosphere should produce a polarization signal of real photons, whose amplitude depends quadratically on the magnetic field strength.

Aims. I search for possible traces of axion-induced low-energy polarization signal in the visible wavelength range.

Methods. I investigate the polarization signal at a continuum wavelength in the visible near 630 nm. I use an observation of a sunspot and the nearby solar active region to study the dependence of the continuum polarization signal on magnetic field strength. I correct the continuum polarization signal for the polarization introduced by the telescope due to oblique reflections. I reproduce the corrected polarization spectra using a spectral synthesis of solar model atmospheres that include the Zeeman effect in the presence of magnetic fields, but no axion-related processes. These synthetic spectra serve as a reference for the amount of polarization from a known source.

Results. I find no trace of an enhanced polarization signal in continuum polarization above a polarization level of around 0.05 %. The continuum polarization and its spatial variation across the field of view at this level can be traced back to either the Zeeman effect or residual cross-talk between intensity and polarization.

Conclusions. I provide a weak upper limit for the existence and interaction of axions with solar magnetic fields by proposing that any model of solar axion generation and interaction should not lead to polarization effects above 0.05 % of the continuum intensity at a wavelength of 630 nm, i.e., not more than 5 out of 10000 photons should show polarization due to axion-related processes. Using estimates of photon and axion flux rates, I derive an upper limit of $g_{a\gamma} < 700 \cdot 10^{-10} \text{ GeV}^{-1}$ for the axion-photon coupling constant $g_{a\gamma}$.

Key words. Sun: Polarimetry – Photosphere

1. Introduction

Comment: The last time this publication was edited was Aug 21, 2008, according to the time-stamp. It was never submitted because of the primarily negative result. At that time, there was a “solar axion telescope” at CERN. I did not look up now if that led to any results.

Axions are hypothetical particles that could constitute a component of the dark matter (see, e.g., Andriamonje et al. 2007, and references therein). Axions can transform into real photons in the presence of magnetic fields with a probability $p_{a \rightarrow \gamma}$ given by

$$p_{a \rightarrow \gamma} = \left(\frac{g_{a\gamma} B}{q} \right)^2 \cdot \sin^2 \left(\frac{qL}{2} \right), \quad (1)$$

where $q = m_a^2/2E$ is the photon-axion momentum difference, $g_{a\gamma}$ the axion-photon coupling and L the extension of the magnetic field with field strength B (taken from Andriamonje et al. 2007). An expansion of the sinus term for $qL \ll 1$ leads to $p_{a \rightarrow \gamma} = 1/2(g_{a\gamma}BL)^2$ (Cameron et al. 1993, Eq. (12)).

The Lagrangian for the interaction of axions and photons contains a scalar product with the magnetic field vector \mathbf{B} , and hence, an anisotropy is introduced in the direc-

tions parallel or perpendicular to the magnetic field direction. This leads to a rotation of linear polarization or the introduction of in general elliptically polarized light (both linear and circular polarized components; Cameron et al. 1993). Axions are assumed to be generated in the solar fusion core. Because of their weak interaction with matter, they can reach the solar surface with little hindrance. The solar surface is, however, known to contain magnetic fields of considerable strength (up to 0.3 T in the center of sunspots) with a large spatial extension (several 10000 kms). A possible interaction of axions generated in the solar core with the surface magnetic fields then should introduce a polarization signal in excess of other known sources of polarization, like the Zeeman effect in solar absorption lines. The additional polarized photons should not be related to specific wavelengths and thus could best be seen in continuum wavelength ranges, where the black-body solar radiation is unpolarized due to the incoherent emission of thermal photons. Any excess continuum polarization in the presence of strong magnetic fields should then also have a quadratic dependence on the field strength (cf. Eq. 1).

To investigate the topic, two quantities have to be determined: the magnetic field strength in the solar atmosphere and the continuum polarization. To this extent, I analyzed a polarimetric observation in the visible wavelength range at 630 nm of an active region on the surface of the Sun. The polarization signature of the magnetic fields due to the

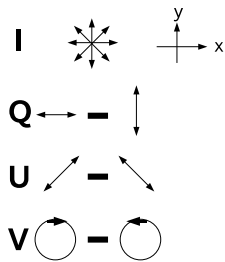


Fig. 1. Graphical sketch of the four Stokes parameters $IQUV$.

Zeeman effect was used to determine the field strength in a two-dimensional (2-D) field of view covering a small and a big sunspot. The continuum polarization was derived from the same data set, which was re-calibrated without the correction for the telescope and the continuum polarization that is part of the usual data reduction. The continuum polarization signal was investigated first in relation to the one predicted by the geometrical model of the telescope that generates continuum polarization by oblique reflections. As second step, the continuum polarization due to the Zeeman effect was studied. Any polarization in excess of these two known sources could be indicative of axion-related processes.

I shortly introduce the telescope, the polarimeter and the data set (Sect. 2). The data reduction procedure is discussed in some detail in Sect. 3, because it is closely related to the question of cross-talk, i.e., the unwanted transformation of polarization states into each other. In Sect. 4, I explain the data analysis procedure and the found behavior and properties of the continuum polarization. The findings are summarized and discussed in Sect. 5.

2. Telescope, polarimeter & observation

In the following study, I will describe the polarization state of the light in the *Stokes formalism* (e.g., Shurcliff 1966; Collett 1992). The polarization state is quantified uniquely by four parameters, commonly combined to the Stokes vector $\mathbf{S} = (I, Q, U, V)$. The four entries correspond to the total intensity, I , the difference of the amount of linear polarization along the x and y axes, Q , the difference of linear polarization at ± 45 degree, U , and the difference of right and left circularly polarized light, V . Figure 1 shows the commonly used graphical representation of the Stokes parameters.

2.1. The German Vacuum Tower Telescope (VTT)

The VTT is a coelostat telescope at the Observatorio del Teide in Izaña, Tenerife (Spain). Two flat 70-cm mirrors are located on top of an eleven-floor tower. The first coelostat mirror, C1, catches the sunlight, the second coelostat mirror, C2, deflects it vertically down into an evacuated steel tube. Inside the steel tube, the main imaging mirror, M3, with a 46-m focal length reflects the light ~ 20 m upwards again to a folding mirror, M4. The folding mirror reflects the light down again. The light beam passes the exit window of the evacuated part after again ~ 20 m. The telescope focus finally is located in the 1st floor of the building. The Instrumental Calibration Unit (ICU) for a calibration of

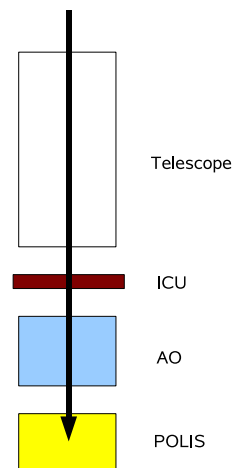


Fig. 2. Schematical light path at the VTT. The light passes the telescope and the AO system before it reaches the polarimeter POLIS. The ICU can be inserted right behind the telescope to calibrate the remaining light path.

polarimeters is located right behind the exit window. In 2003, the Kiepenheuer-Institute adaptive optics (AO) system was installed to improve the spatial resolution by a real-time correction of the wavefront distortions introduced in the earth atmosphere. The corresponding optics are located between the ICU and the polarimeter, as sketched in Fig. 2.

2.2. The Instrumental Calibration Unit (ICU)

The ICU consists of a linear polarizer followed by a retarder. With the ICU, known polarization states can be generated. The instrument response to these known polarization states is measured, and the linear response function can be determined from a comparison between input (known state) and output (measured polarization). The method is described in detail in Beck et al. (2005b) and Beck (2006). The application of the inverse of the response function to the observed Stokes vector corrects all changes of the Stokes vector that were introduced by optics behind the ICU.

2.3. The Polarimetric Littrow Spectrograph (POLIS)

One of the polarimeters at the VTT is the Polarimetric Littrow Spectrograph. The instrument is designed for measurements of the Stokes vector at two *fixed* wavelength ranges in the visible and near-UV (630 nm, 396.8 nm). The instrument uses a rotating waveplate for polarization modulation. The modulated polarization is transformed into a modulated intensity level by polarizing beamsplitters. The polarization state can be reconstructed from the measured variation of the intensity level. The instrument is described in detail in Beck et al. (2005b). I used only the data from the channel at 630 nm, since the near-UV channel was not functional during the observations.

2.4. Data set

For the investigation of the possible existence of axion-induced continuum polarization, an observation taken on the July 6, 2005 was used. Figure 3 shows an overview on

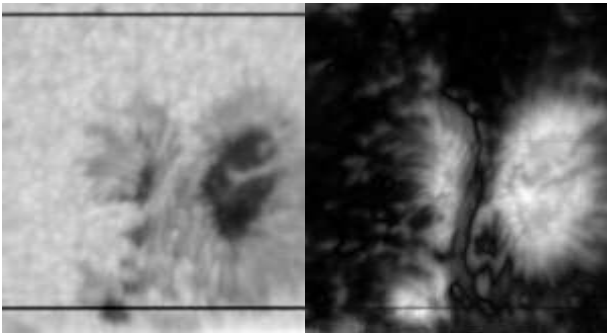


Fig. 3. Overview over the observed field of view. Left: continuum intensity near 630.3 nm. Right: circular polarization signal.

the observed field of view (FOV) in intensity and circular polarization. The FOV covers a big sunspot in the right half, with a clearly discernible dark umbral core and a fully formed penumbra all around the umbral core. A smaller sunspot was located left of it that had a penumbra only in the left-upper part. The *two horizontal black lines* in the intensity map of Fig. 3 are thin wires that were put across the slit to mark the FOV of the CCD camera. Black areas in the circular polarization map can be assumed to be free of magnetic fields to first order. To obtain the 2-D map of the solar surface, the 40 micron wide entrance slit of the spectrograph was stepped across the solar image in the focal plane (“scan”). For each step of the scan, the Stokes vector $IQUV$ of the solar spectrum from around 630.05 nm to 630.4 nm was obtained (cf. Fig. 4). The scanning proceeded from left to right, i.e., the time increases also from left to right. The data set was taken during the time reserved for the International Time Program (ITP), where several telescopes on the Canary islands of Tenerife and La Palma were used in coordinated observations.

3. Standard data calibration procedure

The VTT has not been designed for polarimetry in its very beginning. The telescope is not axi-symmetric and has several oblique reflections on mirrors. Already the first mirror, C1, changes the polarization state significantly and also introduces a time-dependent continuum polarization level at all wavelengths. All oblique reflections anywhere downstream in the light path change again the polarization state. The ICU allows to calibrate the instrument response for all changes of the Stokes vector behind it, but not in front of it. The standard data calibration procedure thus consists of two main steps: a correction for all changes behind (Sect. 3.1) and in front of the ICU (Sect. 3.2).

3.1. Instrument calibration

With the instrument calibration, the polarization measurements are corrected for all changes of the polarization state behind the ICU. The polarimeter response function is determined from the comparison of the polarization states generated with the ICU and the corresponding Stokes vector observed with the instrument. For the instrument calibration, it is not necessary to model the contribution of, e.g., each mirror separately. Only the final net effect on the polarization is determined. The instrument calibration is very

accurate, because the ICU properties are well known and a linear relation between ICU state and measured state can be taken for granted. The method is described in Beck et al. (2005b). The instrument response is determined once per day and shows little to no time dependence, because it reflects the geometry of the light path behind the ICU that is not changing.

3.2. Telescope calibration

No direct calibration is possible for the telescope. To remove the polarization changes due to the telescope, a geometrical model of the telescope is used. It contains the actual light path inside the telescope (C1 to exit window) at any given moment of time. The properties (i.e., the complex refractive index) of the aluminum-coated mirrors were determined by different methods (Beck et al. 2005a; Beck 2006). With the refractive index of the mirrors, the changes of the polarization state due to the oblique reflections on mainly C1 and C2 can be calculated and removed. The telescope calibration is less accurate than the instrument calibration because aging and other degradation (dust, dirt) of the mirror coatings is not taken into account and because the determination of the complex refractive index is only possible within limits. The telescope model has to be calculated for each moment of time with the location of the Sun on the sky and the position and orientation of the mirrors C1 and C2.

3.3. Removal of residual cross-talk

For studies of the polarization signal due to the Zeeman effect, the continuum polarization is commonly assumed to be zero. As both the instrument calibration and the telescope calibration have limitations, the continuum polarization level in calibrated data is usually non-zero. This spurious polarization is produced by cross-talk, i.e., the transformation of one Stokes parameter into another. The main effect is a transformation of intensity, I , into the polarization signals QUV , because for solar light the intensity I is commonly one order of magnitude larger than the polarized fraction, $\sqrt{Q^2 + U^2 + V^2}$. In the standard data reduction, any residual continuum polarization is thus *forced* to zero by subtracting a corresponding fraction of the intensity signal.

4. Data analysis

For the study of the possible continuum polarization induced by axion-related processes, the data set was reduced two times: once the usual standard calibration including the telescope calibration and the removal of residual cross-talk was applied, in the second case only the instrument calibration was applied. The second data sets thus contains both the continuum polarization induced by the telescope, and every other effect that could generate polarization in continuum wavelength ranges. From the observations, one obtains the four Stokes parameters of the spectrum in a small wavelength range (Fig. 4) for each location of the slit during the scan. The spectral range contains two strong solar spectral lines of iron (Fe), and two strong absorption lines of oxygen from the Earth’s atmosphere (O_2). The telluric lines do not show any polarization signal or any measur-

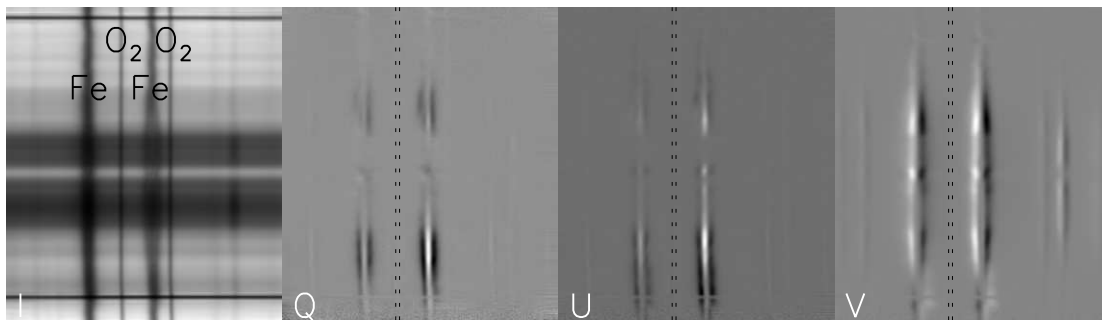


Fig. 4. Spectrum along the slit. *Left to right: IQUV*. Wavelength increases from left to right in each Stokes parameter, the position along the slit from top to bottom. The dashed vertical lines outline the continuum window used throughout the following.

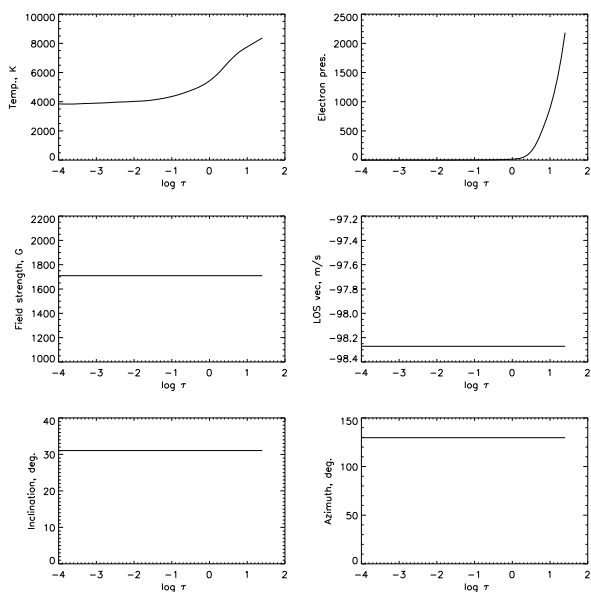


Fig. 5. Solar model atmosphere for the generation of synthetic spectra for one spatial location. *Left column, top to bottom: temperature, field strength, field inclination. Right column: electron pressure (=density), velocity, field azimuth.*

able Doppler shifts due to velocities. The solar lines show the effect of solar magnetic fields due to the Zeeman effect. The spectral lines split into three components in the presence of strong fields (middle of the FOV). Depending on the orientation of the magnetic field lines to the line of sight (LOS) between observer and target, the polarization signal shows up stronger in Q , U , or V (*longitudinal* or *transversal* Zeeman effect).

4.1. Synthetic spectra

To obtain the field strength in the observed FOV, synthetic spectra were generated. The procedure is as follows: one assumes a model for the solar atmosphere. The solar model atmosphere (cf. Fig. 5) contains the thermodynamic properties (temperature, density, velocity), and the magnetic field properties (field strength, field inclination (= angle between field and LOS), field azimuth (= direction of field in the plane perpendicular to the LOS). The model atmosphere is given on grid points in optical depth, $\log \tau$, instead

of a scale in km, because this is fully sufficient for a synthesis of spectra. The spectra resulting from the model atmosphere are calculated. However, they will first not match well to the observed spectra. The properties of the model atmosphere are then iteratively modified in a least-square-fit, until the synthetic spectra match the observed ones. A number of such “inversion¹” codes are available. I used the SIR code (Ruiz Cobo & del Toro Iniesta 1992). The inversion is executed independently for each spectrum (=row of pixels on the CCD) along the slit in every scan step.

Figure 6 shows a comparison of observed and synthetic spectra for two locations in the field of view. The telluric O_2 lines were not included in the synthetic spectra. From the model atmosphere that yields the best-fit spectra one obtains the field strength and field orientation for the solar location where the observed spectra came from. Note that these synthetic spectra *cannot contain* any continuum polarization possibly induced by axions, only the polarization due to the Zeeman effect. The continuum polarization induced by the telescope was also removed prior to the inversion. The synthetic spectra serve as a reference for the continuum polarization signal of known origin, i.e., from the Zeeman effect.

4.2. Continuum polarization induced by telescope and Zeeman effect

Before turning to the spatial variation of the continuum polarization signal, I investigated the polarization level inside the continuum window marked in Fig. 6, averaged along the slit in each scan step. I used the second reduction of the data set where the telescope and residual cross-talk correction was not applied. Figure 7 shows this average continuum polarization as a function of time during the scanning. The *black line* shows the observed continuum polarization. The *red line* is the polarization that is predicted by the telescope model. The *purple line* shows the addition of the polarization in the synthetic spectra plus that of the telescope. The observed and predicted continuum polarization agree satisfyingly, the slope with time predicted by the telescope model is well reproduced. Examining the curve for Stokes V , the locations of the small and the big sunspot can be recognized: the small spot was scanned at around 8.55 UT, the big sunspot at around 8.75 UT, producing an increased and decreased continuum polarization, respectively. The devia-

¹ From spectra to atmosphere is the inverse problem to the generation of the spectra in nature.

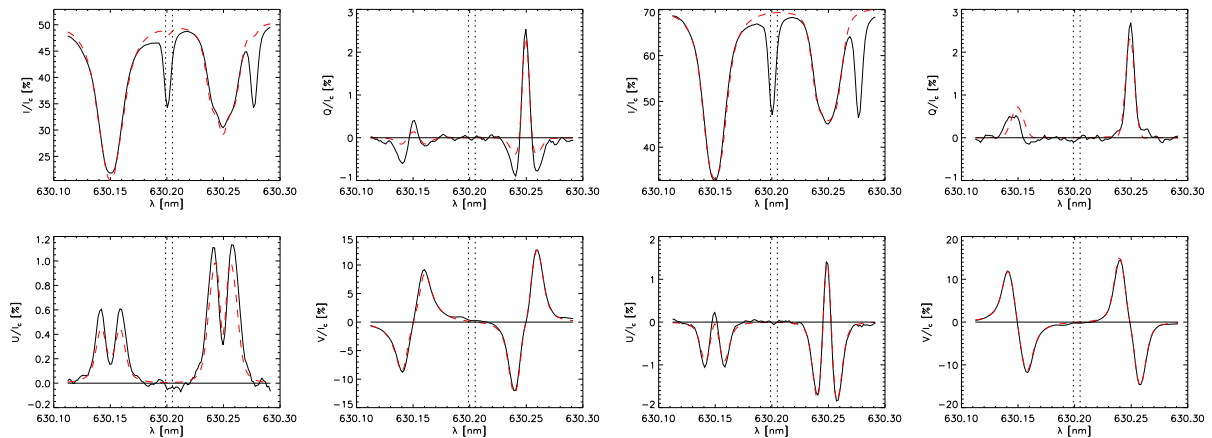


Fig. 6. Observed and synthetic spectra observed on two different spatial locations. *Clockwise, starting left top:* Stokes $IQVU$. *Black solid lines* show the observed profiles, *red dashed* the synthetic spectra. The *dotted vertical lines* outline the continuum window. Note the opposite polarity in the two Stokes V plots (*bottom row, 2nd and 4th column*): the order of maxima and minima of the profile is exchanged, indicating magnetic fields (anti-)parallel to the line of sight.

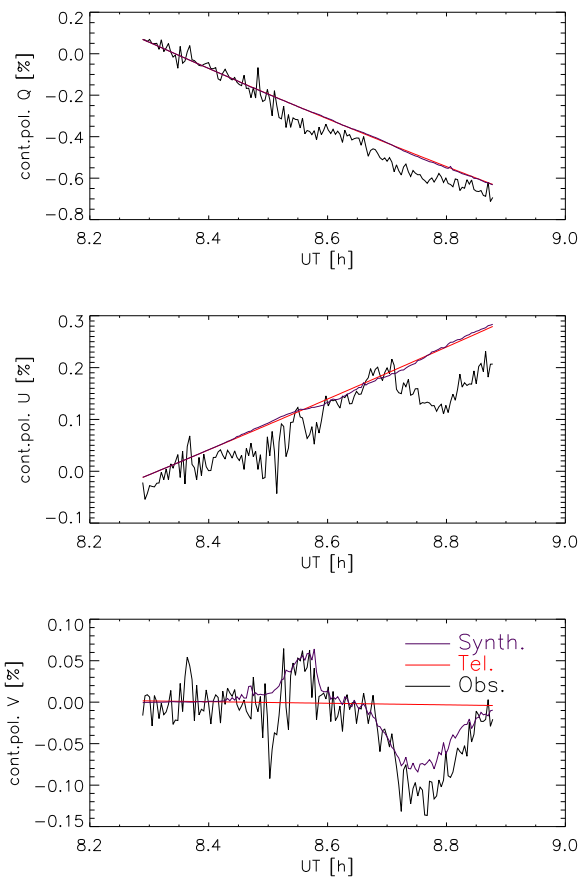


Fig. 7. Continuum polarization induced by the telescope and the Zeeman effect, averaged along the slit. *Top to bottom:* Stokes QUV . *Black:* observed continuum polarization. *Red:* continuum polarization predicted from the telescope model. *Purple:* telescope polarization plus the continuum polarization in the synthetic spectra.

tion in opposite directions is systematic and has an easy explanation.

The circular polarization signal changes its so-called *polarity*, when the magnetic field is parallel or anti-parallel to the LOS. In the spectra, this change is visible as the exchange of the order of maximum and minimum Stokes V polarization signal (cf. Fig. 6). As the Zeeman induced polarization signal extends into the continuum window used to derive the continuum polarization, the change of the polarity leads to a change of the sign of the continuum polarization. This is demonstrated also in Fig. 8. The figure shows histograms of the continuum polarization of all locations with positive and negative polarity, respectively. Positive (negative) polarity is directly related to a positive (negative) continuum polarization signal. In total, the continuum polarization of the synthetic Stokes V spectra (*purple curve* in Fig. 7) shows the same behavior as the observed polarization which implies that this variation is induced by the Zeeman effect. This is not the case for the linear polarizations Q and U : the polarization in the synthetic spectra does not match the observed polarization. The observed deviation from the prediction of the telescope model is much larger than that in the synthetic spectra. This observed variation of the linear polarization is thus not due to the Zeeman effect.

4.3. 2-D maps of the continuum polarization

The previous section has shown that the continuum polarization follows closely the prediction of the telescope model, when no strong magnetic fields are present. This time-dependent contribution to the continuum polarization was thus subtracted from the observed continuum polarization. Figure 9 shows the resulting 2-D maps of the continuum polarization in the observations and in the synthetic spectra, where the spatial variation of the polarization level with the solar surface structure can be seen. I remark once more that the continuum polarization in the synthetic spectra can only be due to the Zeeman effect, because no other processes were considered in the generation of the spectra with the SIR code. For relating the polarization signal to the magnetic field, also the continuum intensity map and the field strength map are shown. As this is the most important figure in the search for a possibly axion-induced

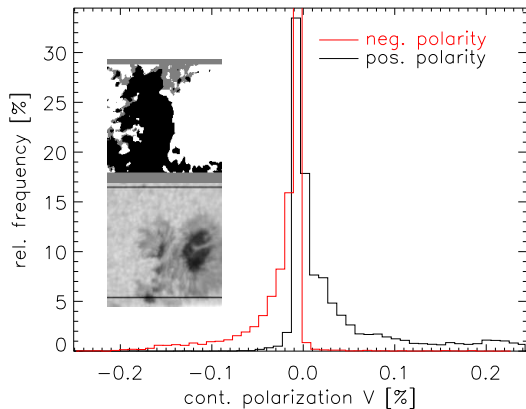


Fig. 8. Histograms of the continuum polarization for locations with positive (*black*) and negative polarity (*red*). Inserted are 2-D maps of polarity (*upper*) and intensity (*lower*) in the left part. *Black* and *white* denote the opposite polarities, *grey* indicates no polarization signal.

continuum polarization, it deserves an extended description, starting with the circular continuum polarization (*3rd column from the left*).

For the circular continuum polarization, the observed and synthetic polarization signals match closely both in the locations and also in the sign of the polarization signal. The strong positive polarization signals (*white*) are restricted to the umbra of the big sunspot, strong negative polarization signals (*black*) appear for the small sunspot and on some locations below it. Outside the contour lines that mark the end of the penumbra for the two sunspots, the polarization level is close to zero. This again indicates that the circular continuum polarization is only due to the Zeeman effect: only for the strong fields in the sunspots the spectral lines split² enough to influence the continuum window.

Stokes Q (*1st column*) shows a different behavior. All areas, which are dark (umbra of big and small sunspot) in the continuum intensity, show increased positive polarization signal. The penumbra shows slightly positive polarization signals. This does not match the polarization signal in the synthetic spectra (*top row*). There the umbra is not prominent in polarization; the maximum is located near the lower part of the big sunspot close to the penumbra. Note that the display range of the synthetic spectra ($\pm 0.05\%$) is smaller by a factor of 5 than that of the observed polarization ($\pm 0.25\%$). Outside the contour lines, the polarization level is close to zero everywhere as for Stokes V .

Stokes U (*2nd column*) differs again from Stokes Q . The observed continuum polarization differs even stronger from the synthetic one than for Stokes Q . The umbra shows again strong positive polarization signal in the observed continuum polarization, but in the penumbra mainly negative continuum polarization is seen. At the left border between the umbra and penumbra of the big sunspot, a ridge of strong negative polarization values is seen (*black color*)³. Contrary to Stokes Q and V , the polarization signals shows a strong spatial variation with a discernible fine structure. Outside the contour lines, the signal level is low, but still

shows spatial structures: several prominent app. circular “blobs” of negative polarization signal can be seen above the two sunspots. The spatial sizes of the “blobs” match that of convection cells, the granulation pattern, which is seen in the intensity map. The brightest areas show a negative polarization signal (dark in continuum polarization), the darkest areas a positive signal (bright). This relation between intensity structures, which are not related to magnetic fields at all, hints at the presence of cross-talk between intensity and Stokes U . In total, the circular polarization signal seems to be induced only by the Zeeman effect and is identical in synthetic and observed spectra, but the linear polarization signal in the observed spectra strongly differs from that of the synthetic ones, like for the average values in the previous section.

4.4. Relation between continuum polarization and field strength

The previous sections have shown that the observed circular continuum polarization is dominated by the Zeeman effect. The observed linear continuum polarization showed strong deviations from the synthetic one. If the linear polarization signal is produced by axion-related processes that are not contained in the synthetic spectra, the signal level should show a dependence on field strength (cf. Eq. (1)) that is known from the inversion of the observed spectra.

Before investigating the relation between field strength and polarization, I turn to the relation between field strength and intensity because this is a crucial point for the later discussion. The energy transport near the solar surface is effected by (overturning) convection rolls: hot material rises vertically (granules), radiates energy away, moves laterally to the side, and sinks down in cool small-scale downdrafts (intergranular lanes). The presence of magnetic fields suppresses convection rolls; the ionized solar plasma cannot cross the field lines. Due to buoyancy forces, solar magnetic fields are mainly vertical to the surface. Thus, inside strong fields no lateral motion is possible and the energy transport is strongly impeded. The material cools and leads to the appearance of dark structures (umbra, penumbra) whenever strong magnetic fields are present⁴.

Figure 10 shows a scatterplot of intensity vs. field strength to visualize their relation. The intensity was normalized to the average intensity in the whole FOV including the dark sunspots. For the locations outside of the sunspots ($I > 1$), in principle any field strength between 0 and 1700 G can appear for a given intensity. For reduced intensities from 0.8 to 1 (penumbra) and 0.4 to 0.8 (umbra), a minimum field strength is required (1000 G and 1700 G, respectively). Intensities below 1 cannot be achieved without magnetic fields.

Keeping the relation between intensity and field strength in mind, one can now turn to the scatterplot of field strength vs. continuum polarization in Fig. 11. For each polarization (QUV), the observed continuum polarization is plotted in *black*, together with that in the synthetic spectra in *red*. Only the absolute value of the continuum polarization is used. I remark that the synthetic spectra are free of noise in contrast to the observations, and hence, have to show slightly lower polarization levels all the time. For

² $\Delta\lambda \propto B$

³ It creates a bit of a 3-D effect.

⁴ If the magnetic field is weak, it is swept away by the lateral flows.

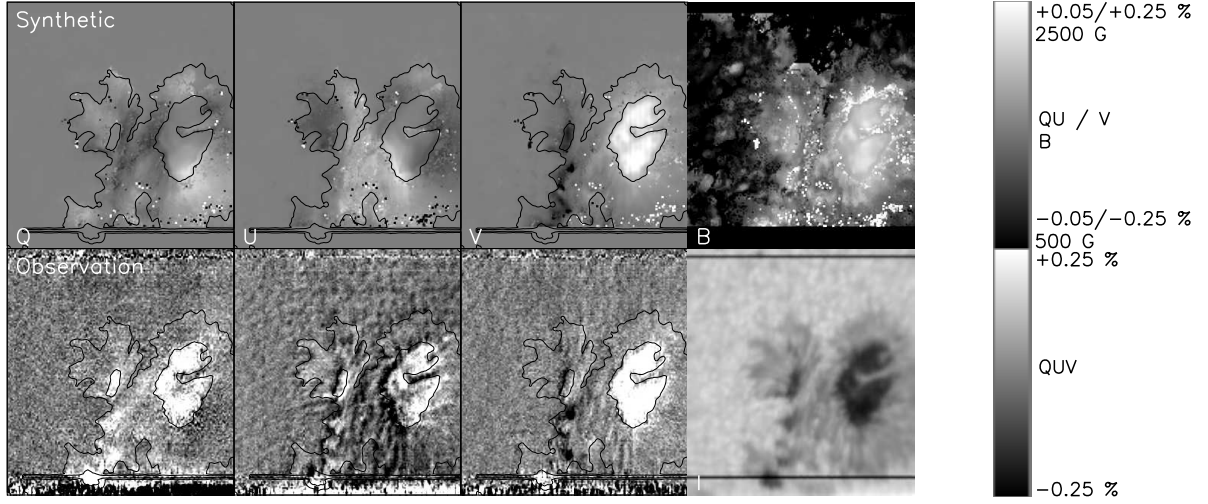


Fig. 9. 2-D map of continuum polarization in the synthetic (*top row*) and observed spectra (*bottom row*). *Left to right: QUV*. *Last column, top: field strength; last column, bottom: Stokes I*. The *black contours* outline the umbra and penumbra of the big and small sunspot.

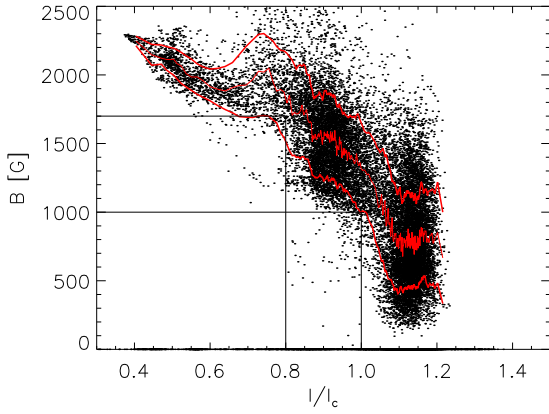


Fig. 10. Scatterplot of continuum intensity (I_c) vs. field strength (B). The *vertical and horizontal lines* mark two steps in the relationship: if the intensity is below 1, the fields are generally above 1000 G (penumbra), if the intensity is below 0.8, the fields are above 1700 G (umbra). The *red lines* denote the average value and its standard deviation.

Stokes V , again a reasonable agreement is seen: both synthetic and observed polarization increase with field strength for field strengths above 1500 G. For the linear polarizations Q and U , the synthetic polarization is always as good as zero, regardless of field strength. The linear polarization in the observation, however, shows increased continuum polarization signal for field strengths above 1700 G, as would be expected from also Fig. 9: the umbra has strong fields and shows increased linear continuum polarization.

5. Summary & Discussion

The average observed continuum polarization follows the prediction of the telescope model closely, when no magnetic fields are present. This indicates that the measurements can be trusted down to a polarization level of around 0.05 %. The strong magnetic fields of the sunspots inside the field of view show up both in the averaged continuum

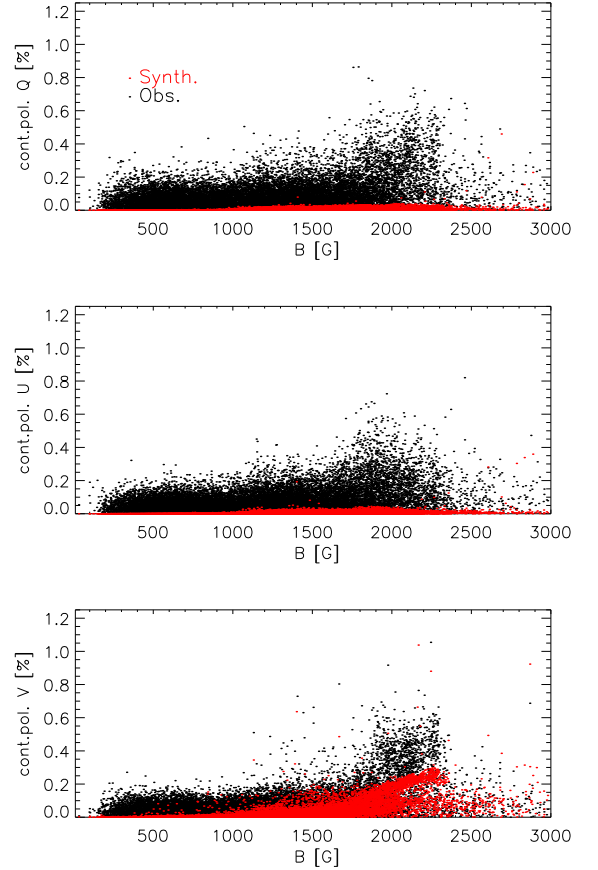


Fig. 11. Scatterplot of field strength vs. continuum polarization. *Top to bottom: QUV*. *Black: observed spectra. Red: synthetic spectra*.

polarization as well as in spatially resolved 2-D maps. The *circular continuum polarization* is found to be mainly *due to the Zeeman effect* in the presence of magnetic fields. In any comparison of the observed circular continuum polarization with that in synthetic spectra generated including

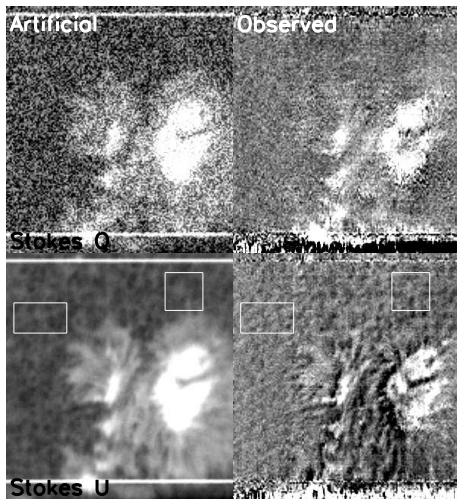


Fig. 12. Comparison of artificially constructed maps of continuum polarization (*left column*) with the observed continuum polarization (*right column*). *Top row*: Stokes Q . *Bottom row*: Stokes U . The *white rectangles* outline areas, where spatial structures can be well seen in artificial and observed map.

only the Zeeman effect, a nearly perfect agreement is found (Figs. 7 and 9). The change of the sign of the observed circular continuum polarization between the big and small sunspot inside the field of view can be directly traced back to the change of the polarity in the Stokes V spectra.

For the linear polarization, the continuum polarization in the observed and synthetic spectra does not match. The umbra of the spots shows stronger continuum polarization signal in the observed spectra, whereas the synthetic spectra predict a maximum polarization outside of the umbra. In the observed continuum polarization of Stokes U , spatial structures can be discerned outside the sunspot. They resemble the granulation pattern seen in the intensity map, i.e., they are not related to the spatial distribution of magnetic fields but of intensity. The scatterplot of field strength vs. the continuum polarization shows an increase of the continuum polarization for strong magnetic fields above 1700 G.

It can, however, be demonstrated that the enhanced linear polarization signal is *not* related to axions but residual cross-talk from intensity into the linear polarization. The appearance of the granulation/intensity pattern in the observed Stokes U continuum polarization already is a clear indication of that. The prominent appearance of the sunspot(s) in the polarization maps also is no problem: the intensities in the umbra and penumbra are around 0.4 and 0.8 of the average intensity, respectively. Any linear relation between intensity and polarization thus will lead to a prominent signature of the sunspots in polarization. To demonstrate that the observed continuum polarization is due to residual cross-talk, I generated two artificial continuum polarization maps from the continuum intensity map, I , by:

$$P_{\text{art}} = -0.007 \cdot I + \epsilon, \quad (2)$$

where ϵ is an added random noise contribution, and P_{art} stands for Stokes Q and Stokes U , respectively. For Stokes U , the noise was chosen to have around 4 % of the signal amplitude, for Stokes Q around 50 %.

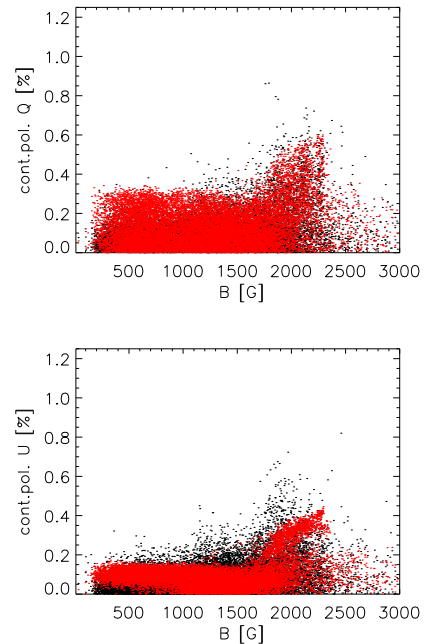


Fig. 13. Scatterplot of field strength vs. continuum polarization. *Top to bottom*: QU . *Black*: observed spectra. *Red*: artificial continuum polarization maps.

Figure 12 shows the artificial continuum polarization maps thus obtained, together with the observed continuum polarization maps. The artificial maps show the inverted intensity structure due to the minus sign in their generation, which was prompted by the anti-correlation between intensity and linear continuum polarization signal. The spatial structures in the observed Stokes U continuum polarization can be found one-to-one again in the artificial map. The reduced polarization signal (*black*) at the umbra-penumbra boundary at the left side of the big spot appears also in the artificial map, even if it is less prominent there. Several of the “blobs” (=granules) outside the spot can be directly identified with their counterpart in the artificial map. Two rectangles highlight areas, where the correspondence can best be seen. In the left one, an app. straight line of increased polarization signal crosses the rectangle from the lower left to the upper right corner in the artificial map. The same line is faintly visible in the observed continuum polarization map. In the second rectangle, a larger blob of increased signal is located around the center. It appears again in the observed continuum polarization map. As final test, the same scatterplot of field strength vs. continuum polarization as in Fig. 11 was done for the artificial maps (Fig. 13). Especially for Stokes Q , the observed and artificial polarization signal are indistinguishable, including the increase of polarization for large field strengths. The noise level in the artificial Stokes Q map was chosen a bit too high, but that has no consequences on the conclusions.

From the comparison with the synthetic spectra and the reproduction of the spatial distribution of the linear continuum polarization by cross-talk from I into Q and U , I would exclude the presence of excess unexplained (possibly axion-related) polarization signal above a level of around 0.05 % of I_c , or 5 out of 10000 photons. This limit in polarization degree translates, however, only into a very weak

upper limit for the axion-photon coupling due to the large number of photons that are present from the solar black-body radiation. The number of axion-related photons, γ_{ax} , would be given by

$$\gamma_{ax} = p_{a \rightarrow \gamma} n_{ax} , \quad (3)$$

where n_{ax} is the number of axions at the solar surface. Andriamonje et al. (2007) give a value of around $\phi_a = g_{10} \cdot 10^{15} \text{ m}^{-2} \text{ s}^{-1} \text{ keV}^{-1}$ for the solar surface axion flux, with $g_{10} = g_{a\gamma} / 10^{-10} \text{ GeV}^{-1}$.

Using the approximation of Cameron et al. (1993), $p_{a \rightarrow \gamma}$ is proportional to $(g_{a\gamma} BL)^2$. The continuum radiation comes only from a small layer in the solar atmosphere with around 50-200 km vertical extension. Using an upper limit of $B = 0.2 \text{ T}$ and $L = 200 \text{ km}$, $(BL)^2 \sim 10^9 \text{ (Tm)}^2$. This gives an axion-related photon flux, $\phi_{\gamma,a}$ of

$$\phi_{\gamma,a} = \phi_a \cdot p_{a \rightarrow \gamma} \sim (g_{10})^3 \cdot 10^{24} \text{ m}^{-2} \text{ s}^{-1} \text{ keV}^{-1} . \quad (4)$$

The additional polarization signal would be given by the fraction of axion-related photon flux to that from the unpolarized black-body (bb) radiation, γ_{bb} . With a solar surface temperature of 5800 K, the Planck curve predicts a power of $p = 7.5 \cdot 10^{10} \text{ Wm}^{-2} \text{ nm}^{-1}$ near 630 nm. The continuum window used extends over around 0.01 nm, and the energy of a single photon at 630 nm is around $3 \cdot 10^{-19} \text{ J}$ ($\sim 2 \text{ eV}$). The radiation power then transforms into a photon flux from the black-body radiation of

$$\phi_{\gamma,bb} = 7.5 \cdot 10^{10} \cdot 0.01 / 3 \cdot 10^{-19} = 2.4 \cdot 10^{27} \text{ m}^{-2} \text{ s}^{-1} . \quad (5)$$

Assuming that the axion-flux in the eV range is at least an order of magnitude lower than near its maximum at around 3 keV (Andriamonje et al. 2007, their Fig. 2) and transforming the extension of the continuum window in the spectrum into an energy interval of $3 \cdot 10^{-5} \text{ eV}$, yields

$$\phi_{\gamma,a} = (g_{10})^3 \cdot 3 \cdot 10^{15} \text{ m}^{-2} \text{ s}^{-1} . \quad (6)$$

With the observed upper limit that less than $5 \cdot 10^{-4}$ of the photons in the continuum window show additional polarization signal from possibly axion-related processes, it follows that

$$\begin{aligned} (g_{10})^3 &< 5 \cdot 10^{-4} \cdot 2.4 \cdot 10^{27} / 3 \cdot 10^{15} = 4 \cdot 10^8 \\ \text{or } g_{10} &< 700 . \end{aligned} \quad (7)$$

6. Conclusion

The final result of this investigation is a negative one: there are no traces for axion-induced polarization signals in a continuum wavelength near 630 nm above a level of around 0.05 % of I_c . The residual linear continuum polarization signal at locations of strong magnetic fields could be shown to be due to cross-talk from intensity into polarization. This leads⁵ to a value of the axion-photon coupling $g_{a\gamma} < 700 \cdot 10^{-10} \text{ GeV}^{-1}$. Andriamonje et al. (2007) exclude a value of $g_{a\gamma} > 4.5 \cdot 10^{-10} \text{ GeV}^{-1}$, which is some orders of magnitude below the present estimate. The present

method of estimating $g_{a\gamma}$ could be improved by observations with a significant better S/N ratio, produced by much longer exposure times, or large-scale spatial averaging over, e.g., the whole umbra and penumbra of a spot. In addition, the active region was off the center of the solar disk by >10 degrees. Solar axions should only induce real photons in forward scattering, so observations of an active region closer to or best directly at disc center would be preferred.

Acknowledgements. I thank K.Zioutas for providing the idea for this study. The VTT is operated by the Kiepenheuer-Institut für Sonnenphysik (KIS) at the Spanish Observatorio del Teide of the Instituto de Astrofísica de Canarias (IAC). The POLIS instrument has been a joint development of the High Altitude Observatory (Boulder, USA) and the KIS.

References

- Andriamonje, S., Aune, S., Autiero, D., et al. 2007, Journal of Cosmology and Astro-Particle Physics, 4, 10
- Beck, C. 2006, PhD thesis, Albert-Ludwigs-University, Freiburg
- Beck, C., Schlichenmaier, R., Collados, M., Bellot Rubio, L., & Kentischer, T. 2005a, A&A, 443, 1047
- Beck, C., Schmidt, W., Kentischer, T., & Elmore, D. 2005b, A&A, 437, 1159
- Cameron, R., Cantatore, G., Melissinos, A. C., et al. 1993, Phys. Rev. D, 47, 3707
- Collett, E. 1992, Polarized light. Fundamentals and applications (Optical Engineering, New York: Dekker)
- Ruiz Cobo, B. & del Toro Iniesta, J. C. 1992, ApJ, 398, 375
- Shurcliff, W. A. 1966, Polarized light. Production and use (Cambridge, Mass.: Harvard University Press)

⁵ In this estimate it is assumed that an axion of energy E produces a photon of the same energy, but I don't know if that is to be expected. I'm also not fully sure about units, but Cameron et al. (1993) give $(g_{a\gamma} BL)^2$ as a unitless probability. I hope this comes out naturally using SI units for B and L .